MOLECULAR AND CELLULAR BIOLOGY, July 2001, p. 4119–4128 Vol. 21, No. 13
0270-7306/01/$04.00+0 DOI: 10.1128/MCB.21.13.4119–4128.2001

Loss of Annexin A7 Leads to Alterations in Frequency-Induced Shortening of Isolated Murine Cardiomyocytes

CLAUDIA HERR,[1] NEIL SMYTH,[2] SUSANNE ULLRICH,[3] FAN YUN,[3] PHILLIP SASSE,[3] JÜRGEN HESCHELER,[3] BERND FLEISCHMANN,[3] KATRIN LASEK,[4] KLARA BRIXIUS,[4] ROBERT H. G. SCHWINGER,[4] REINHARD FÄSSLER,[5] ROLF SCHRÖDER,[6] AND ANGELIKA A. NOEGEL[1]*

Institute of Biochemistry I[1] and II,[2] Department of Neurophysiology,[3] and Laboratory of Muscle Research and Molecular Cardiology, Clinic III of Internal Medicine,[4] University of Cologne, 50931 Cologne, and Department of Neurology, University Hospital Bonn, Bonn,[6] Germany, and Department of Experimental Pathology, Lund University, Lund, Sweden[5]

Received 21 December 2000/Returned for modification 1 February 2001/Accepted 6 April 2001

Annexin A7 has been proposed to function in the fusion of vesicles, acting as a Ca^{2+} channel and as Ca^{2+}-activated GTPase, thus inducing Ca^{2+}/GTP-dependent secretory events. To understand the function of annexin A7, we have performed targeted disruption of the *Anxa7* gene in mice. Matings between heterozygous mice produced offspring showing a normal Mendelian pattern of inheritance, indicating that the loss of annexin A7 did not interfere with viability *in utero*. Mice lacking annexin A7 showed no obvious phenotype and were fertile. To assay for exocytosis, insulin secretion from isolated islets of Langerhans was examined. Ca^{2+}-induced and cyclic AMP-mediated potentiation of insulin secretion was unchanged in the absence of annexin A7, suggesting that it is not directly implicated in vesicle fusion. Ca^{2+} regulation studied in isolated cardiomyocytes, showed that while cells from early embryos displayed intact Ca^{2+} homeostasis and expressed all of the components required for excitation-contraction coupling, cardiomyocytes from adult *Anxa7*$^{-/-}$ mice exhibited an altered cell shortening-frequency relationship when stimulated with high frequencies. This suggests a function for annexin A7 in electromechanical coupling, probably through Ca^{2+} homoeostasis.

Annexins are a family of Ca^{2+}-and phospholipid-binding proteins encoded by at least 12 different genes in mammals and by numerous other genes in invertebrates and plants. They are characterized by a bipartite structure with a variable N-terminal domain and a conserved C-terminal core. The latter is formed by either four- or eightfold repeats of approximately 70 amino acids, each repeat carrying a Ca^{2+}-binding site. This C-terminal domain is also responsible for phospholipid binding. The unique N-terminal regions are thought to confer functional diversity (35). Although annexins have been well characterized structurally and biochemically, their cellular importance is unclear. Several roles have been proposed, such as the inhibition of phospholipase A2 and of blood coagulation (36, 48), the aggregation of chromaffin granules (10), cross-linking functions in the cell cortex (13), endo- and exocytosis (1, 11), as well as functioning in the regulation and formation of ion channels (18).

Annexin A7 (also called synexin), the first family member to be described, was isolated as the agent that mediated aggregation of chromaffin granules and fusion of membranes and phospholipids (8). Annexin A7 is unusual in that it carries a long N-terminal extension of more than 100 amino acids. Alternative splicing may lead to the inclusion of an extra exon in this region and leads to the generation of two isoforms of 47 and 51 kDa. The 47-kDa protein is present in all tissues except for skeletal muscle. Here the 47-kDa form is lost upon myoblast differentiation, with the 51-kDa isoform being exclusively present in myotubes (6, 38). Both forms are expressed in the heart and brain (24, 38).

As with other family members, the function of annexin A7 remains unclear. There are reports of it acting as a Ca^{2+} channel and as Ca^{2+}-activated GTPase, supporting Ca^{2+}/GTP-dependent secretion (5). Annexin A7 is found in the vicinity of secretory vesicles, on subcellular membranous structures, and on plasma membranes (6, 22), suggesting a possible role in Ca^{2+}-mediated exocytosis. However, in spite of these properties, it has been difficult to unambiguously establish its function. Srivastava et al. recently described an annexin A7 knockout mouse in which its absence resulted in lethality at embryonic day (E10) due to cerebral hemorrhaging; further, heterozygous mice had defects in inositol 1,4,5-triphosphate (IP_3) receptor expression, Ca^{2+} signaling, and a lowered insulin content in the endocrine pancreas (39).

To describe further its in vivo function, annexin A7-deficient (*Anxa7*$^{-/-}$) mice were generated by homologous recombination in embryonic stem (ES) cells. The resulting *Anxa7*$^{-/-}$ mice are viable, are fertile, and exhibit no differences from wild-type (WT) animals with respect to insulin production and secretion. However, while no abnormalities in Ca^{2+} homeostasis are seen at the early embryonic stage, adult mice display defects in cardiomyocyte function.

MATERIALS AND METHODS

Construction of an *Anxa7* targeting construct. An EMBL3 mouse genomic library of the 129SV mouse line (46) was screened with a full-length mouse *Anxa7* cDNA as a probe. A 15-kb genomic fragment, containing exons 4 to 13, was used to generate the targeting vector in pBluescript SK. A *Mun*I site in intron 4 was deleted by partial digestion and religation. The sequences were then interrupted at the remaining *Mun*I site in exon 8 by insertion of the neomycin resistance (*neo*) cassette from plasmid pPNT, resulting in the targeting vector

* Corresponding author. Mailing address: Institute of Biochemistry I, Joseph-Stelzmann-Str. 52, 50931 Cologne, Germany. Phone: 49 221 478 6980. Fax: 49 221 478 6979. E-mail: noegel@uni-koeln.de.

pM1P:BS. Exon 8-encoded amino acids are located at the start of the annexin core domain. In this plasmid, the *neo* cassette divided the *Anxa7* fragment into two arms, with 5 kb of homology in the 5′ arm and 10 kb in the 3′ arm. The *neo* cassette was inserted so as to be transcribed in the opposite orientation to the annexin A7 gene. Finally, plasmid pM1P:BS was linearized with *Cla*I prior to transfection.

***Anxa7* gene targeting in ES cells.** D3 mouse ES cells (9) were grown in standard ES conditions with Dulbecco modified Eagle medium supplemented with 15% fetal bovine serum, 0.1 mM β-mercaptoethanol, and 1,000 U of leukemia inhibitory factor (ESGRO; Life Technologies) per ml. Then 10^7 cells were transfected by electroporation with 25 μg of linearized pM1P:BS, and colonies were selected for resistance to G418 at 350 μg/ml in the culture medium. Surviving clones were picked and expanded, and DNA was extracted for Southern blot analysis. DNA from the cells was probed with an external 5′ probe and an internal 3′ probe. In the case of correct integration, the WT 13-kb *Eco*RI fragment was increased to 15 kb.

Production of *Anxa7*$^{-/-}$ mice. Two independent ES cell lines were used to generate germ line chimeras. Blastocysts were isolated from C57BL/6 mice 3.5 days postcoitum and were injected with 10 to 15 *Anxa7*$^{+/-}$ ES cells. Blastocysts were then transferred into uteri of pseudopregnant foster mothers. Chimeric male progeny were mated to C57BL/6 females, and offspring were tested for germ line transmission by Southern blots of DNA extracted from tail biopsies. Heterozygous animals were mated together to establish a breeding colony.

Western blot and RNA analyses. For Northern blot analysis, total RNA was extracted from brain, heart, liver, and skeletal muscle tissues with TRIzol reagent (Gibco-BRL). Then 30 μg of total RNA was separated on a formaldehyde gel (1% agarose), transferred to a nylon membrane (Biodyne; Pall), and probed with *Anxa7* cDNA and the *neo* cassette.

Gene expression studies were done using DNA microarrays (mouse Gem2; Incyte Genomics, Palo Alto, Calif.). They were hybridized with poly(A) RNA from heart, brain, and pancreas tissues of WT and *Anxa7*$^{-/-}$ mice, and levels of annexins A1, A3 to A7, A10, and A11 were analyzed.

For Western blot analysis, cell extracts prepared from brain, heart, liver, pancreas, and skeletal muscle tissues were electrophoresed in a sodium dodecyl sulfate (SDS)–12% polyacrylamide gel and transferred onto nitrocellulose (Schleicher & Schuell, Dassel, Germany). Membranes were probed as described previously (6) with antibodies against annexins A1 (mouse monoclonal antibodies), A2 (rabbit polyclonal sera), A6 (sheep polyclonal sera) (all kindly provided by V. Gerke), A5 (mouse monoclonal antibodies; kindly provided by M. Kawaminami), A11 (human autoantibody sera, kindly provided by W. van Venrooij), and A7 (mouse monoclonal antibodies 203–217 and 203–80, detecting different epitopes) (38) and a polyclonal rabbit anti-annexin A7 serum raised against the recombinant full-length protein. Protein bands were detected by chemiluminescence.

Two-dimensional gel electrophoresis. Protein separation was carried out by two-dimensional gel electrophoresis (14, 28). Briefly, tissue samples were homogenized in lysis buffer and centrifuged (100,000 × *g*, 1 h). For Western blot analysis, 200 μg of total protein was applied on Immobiline DryStrips (pH 3 to 10; Pharmacia) by in-gel rehydration. The first dimension was run on a Multiphor chamber (Pharmacia) for 10,000 V · h. Separation in the second dimension was carried out in an SDS–12% polyacrylamide gel; proteins were then transferred to nitrocellulose and probed as described previously (6).

Histological analysis. For general histological analysis, organs were dissected, fixed in paraformaldehyde, embedded in paraffin, and sectioned at 7 μm. Sections were then stained with hematoxylin and eosin. Muscles were frozen in liquid nitrogen-cooled isopentane and sectioned at 7 μm. For microscopy, sections were stained either with hematoxylin and eosin, with trichrome according to the method of Gomori, with oil red, by the periodic acid-Schiff reaction, or for different specific enzymes (cytochrome *c* oxidase, succinate dehydrogenase, NADH, and alkaline phosphatase).

Cell dissociation of early embryonic cardiomyocytes. Murine embryos (E11.5 to E12.5) were obtained from *Anxa7*$^{-/-}$ and control mice by using standard superovulation protocols (12). Embryonic hearts were dissected and enzymatically digested as described before (20). Contracting cardiomyocytes were used in the experiments described below.

Ca^{2+} imaging. Ca^{2+} imaging experiments were performed as described previously (21). Briefly, isolated murine cardiomyocytes were incubated for 12 min in the cell-permeable dye fura-2AM (2 μM; Molecular Probes, Eugene, Oreg.) at 37°C and then washed for 5 min. Excitation light (340/380 nm) was applied using a monochromator at frequencies ranging from 2 to 5 Hz. The emitted fluorescence from the fura-2AM-loaded cells (>470 nm) was monitored using a charge-coupled device cooled camera (TILL Photonics, Planegg, Germany). The emission data were analyzed using the Vision software package (TILL Photonics). Results are displayed as 340/380 nm ratios after background subtraction. The extracellular solution consisted of 140 mM NaCl, 5 mM KCl, 2 mM $CaCl_2$, 2 mM $MgSO_4$, 5 mM HEPES 5, and 10 mM glucose (pH 7.4, adjusted with NaOH); the high-K^+ solution consisted of 5 mM NaCl, 140 mM KCl, 2 mM $CaCl_2$, 2 mM $MgSO_4$, 5 mM HEPES, 10 mM glucose (pH 7.4, adjusted with KOH).

Electrophysiology. Patch clamp recordings were performed as described before (21). Briefly, cells were held in the voltage-clamp or current-clamp mode using an EPC-9 amplifier (Heka, Lambrecht, Germany). For the recording of Ca^{2+} current (I_{Ca}), voltage-clamped cells were held at −50 mV, and trains of depolarizing pulses lasting 50 ms were applied to a test potential of 0 mV at a frequency of 0.2 Hz. Current-voltage relationships were determined by applying 150-ms depolarizing voltage steps from test potentials of −40 to 40 mV in 10-mV steps (holding potential of −50 mV). Results are expressed as means ± standard errors of the means (SEM). Statistical analysis was performed using unpaired Student's *t* test, and a probability value of <0.05 was considered significant. For current-clamp and ramp depolarization recordings, the internal solution consisted of 50 mM KCl, 80 mM potassium aspartate, 1 mM $MgCl_2$, 3 mM MgATP, 10 mM EGTA, and 10 mM HEPES (pH 7.4, adjusted with KOH), and the external solution consisted of 140 mM NaCl, 5.4 mM KCl, 3.6 mM $CaCl_2$, 1 mM $MgCl_2$, 10 mM HEPES, and 10 mM glucose (pH 7.4, adjusted with NaOH). For voltage-clamp recordings, the internal solution consisted of 120 mM CsCl, 3 mM $MgCl_2$, 5 mM MgATP, 10 mM EGTA, and 5 mM HEPES 5) (pH 7.4, adjusted with CsOH), and the external solution consisted of 120 mM NaCl, 5 mM KCl, 3.6 mM $CaCl_2$, 20 mM TEA-Cl, 1 mM $MgCl_2$, and 10 mM HEPES (pH 7.4, adjusted with TEAOH). Carbachol (CCh) and caffeine were purchased from Sigma (Deisenhofen, Germany), dissolved in the extracellular solution, and stored frozen at −20°C. Aliquots were thawed immediately before use and diluted to the desired concentration in the bath solution.

Isolation and preparation of adult cardiomyocytes. Ventricular myocytes were prepared from 10- to 12-week-old WT ($n = 8$) and *Anxa7*$^{-/-}$ ($n = 7$) mice. In brief, the heart was quickly excised, and the aorta was cannulated to the base of a Langendorff column (height, 1.0 m). After an initial 10-min perfusion period with Ca^{2+}-free Tyrode's solution (11.1 mM glucose, 10 mM HEPES-NaOH, 5.8 mM KCl, 0.9 mM $MgSO_4$, 0.4 mM NaH_2PO_4, 0.5 mM KH_2PO_4, 140 mM NaCl [pH 7.1, 37°C]), the heart was perfused for 15 to 25 min with Ca^{2+}-free Tyrode's solution containing collagenase (type I; 1 mg/ml; Sigma). Ca^{2+} was added every 3 to 5 min to the solution until a final concentration of 100 μmol/liter was reached. To wash out the collagenase, hearts was perfused for 10 min with a solution consisting of 30.0 mM KCl, 30.0 mM KH_2PO_4, 50.0 mM glutamate, 20.0 mM taurine, 10 mM glucose, 0.5 mM EGTA, and 3 mM $MgSO_4$ (pH 7.3, adjusted with KOH). The ventricles were separated from the atria, and ventricular cells were mechanically dispersed in the glutamate solution. Myocytes were stored for 30 min at room temperature before use.

Measurement of cell contraction. Experiments were performed at 32°C in Tyrode's solution (2 mM $CaCl_2$, 120 mM NaCl, 5.4 mM KCl, 1 mM $MgCl_2$, 22.6 mM $NaHCO_3$, 0.42 mM NaH_2PO_4, 5 mM glucose, 0.3 mM ascorbic acid, 0.05 mM EDTA [pH 7.4, carbogen gassed]). Aliquots (400 μl) of the cell suspension were placed on laminin-coated glass cover slips forming the bottom of the chamber and allowed to adhere at room temperature. Measurements were taken with an inverted microscope as previously described (17).

Isolation and incubation of Langerhans islets. After isolation by collagenase digestion (1 mg/ml; Serva, Heidelberg, Germany), purified islets were preincubated for 1 h at 37°C in incubation buffer containing, per liter, 140 mmol of NaCl, 5.6 mmol of KCl, 1.2 mmol of $MgCl_2$, 2.6 mmol of $CaCl_2$, 2.8 mmol of glucose, 10 mmol of HEPES (pH 7.4), and 5 g of bovine serum albumin (fraction V; Sigma). Thereafter, batches of 10 islets per ml were incubated for 30 min at 37°C in the presence of test substances as indicated for each experiment. Insulin released into the supernatant and the insulin content of the islets after acid-ethanol (1.5%/75% [vol/vol]) extraction were measured by radioimmunoassay as described previously (42).

For perfusion experiments, 100 islets were placed in a column containing 200 mg of Biogel P-2 (Bio-Rad, Munich, Germany), and incubation buffer containing 2.8 mmol of glucose per liter was circulated over the column at 0.7 ml/min for 1 h at 37°C. Incubation was started by adding the test substances at appropriate concentrations, and samples were collected every minute. Results are presented as mean ± SEM. Statistical significance was determined by Student's *t* test for paired and unpaired observations. The level of statistical significance was set at a probability of 0.05.

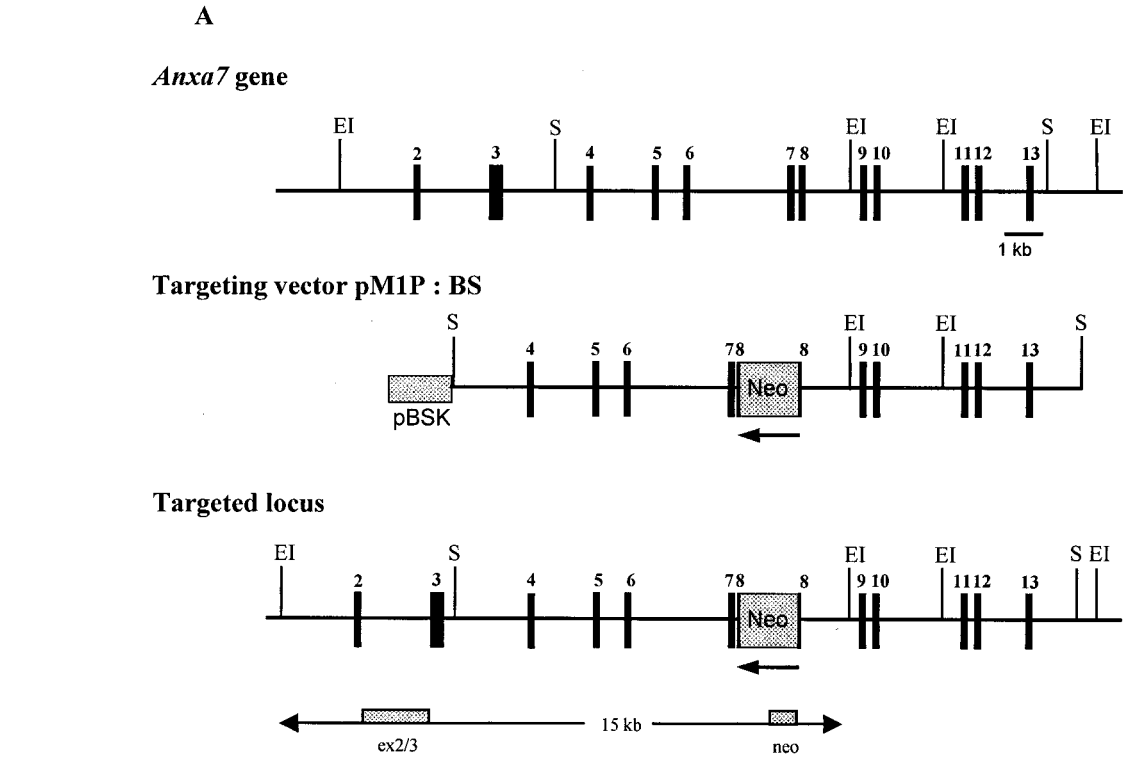

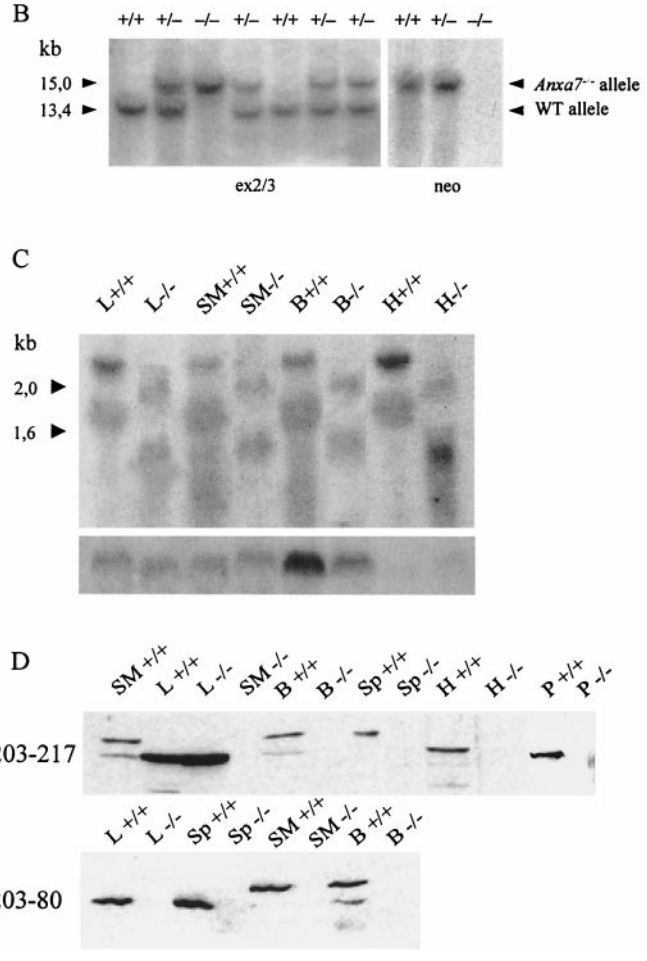

FIG. 1. Targeted inactivation of the *Anxa7* gene. (A) The murine *Anxa7* gene (top) consists of 14 exons (black bars), with exon 14 containing 3′ untranslated sequences. Disruption of *Anxa*7 was achieved by targeting the phosphoglycerate kinase-*neo* cassette to exon 8 (targeting vector pM1B:BS). Lines represent intronic sequences. EI, *Eco*RI, S, *Sal*I. (B) Southern blot analysis of mouse tail DNA digested with *Eco*RI and analyzed using the 5′ external probe ex2/3 or *neo* probe. The external ex2/3 probe detects a 15-kb fragment (targeted allele) or a 13-kb fragment (WT allele); the *neo* probe detects the 15-kb targeted band. (C) Northern blot analysis of different organs from WT and homozygous *Anxa7*$^{-/-}$ animals. Transcripts of 2.4 and 1.8 kb corresponding to the normal *Anxa7* mRNAs are detected in the WT samples; smaller transcripts of 1.9 and 1.5 kb are detected in the knockout samples. The β-actin control is shown below. (D) Western blot analysis of homogenates from different organs from WT and *Anxa7*$^{-/-}$ mice with antibodies 203–217 and 203-80. Antibody 203–217 detects a 47-kDa protein in the liver of *Anxa7*$^{-/-}$ mice which could not be detected by 203-80. B, brain; H, heart; L, liver; P, pancreas; SM, skeletal muscle; SP, spleen.

RESULTS

Generation of *Anxa7*$^{-/-}$ mice. D3 ES cells were electroporated with the targeting vector pM1P:BS (Fig. 1A). Ten of 700 G418-resistant ES cell clones underwent homologous recombination at the *Anxa7* locus, as determined by Southern blot analysis (data not shown). Targeted cells were injected into host C57BL/6 blastocysts, which were transferred into the uteri of pseudopregnant females. Resulting chimeric animals were used to derive heterozygous offspring. These did not display any obvious abnormalities in comparison to their WT littermates.

***Anxa7*$^{-/-}$ mice are viable and fertile.** To examine whether homozygous mutant animals were viable, we intercrossed heterozygotes and determined the genotypes of their offspring by

Southern blot analysis. Mice homozygous for the *anxa7* mutation, with loss of the 13-kb WT band and the appearance of a 15-kb band, were detected (Fig. 1B). Pups from 36 such litters were genotyped in this way, and the ratio of +/+, +/−, and −/− mice (28%: 48%: 24%) reflected the predicted Mendelian ratios of 1:2:1 for nonlethal alleles. Homozygous *Anxa7*$^{-/-}$ mice were indistinguishable from their WT littermates on the basis of size, activity, fertility, or aging. Interbred *Anxa7*$^{-/-}$ females produced normal litter sizes.

As described previously (24), Northern blot analysis revealed two mRNAs of 2.4 and 1.8 kb in WT mice. The two transcripts are due to different poly(A) signals and were detectable with an N- and a C-terminal cDNA *Anxa7* probe. In *Anxa7*$^{-/-}$ mice, two mRNAs of 1.9 and 1.5 kb were recognized by the C-terminal probe (Fig. 1C). The N-terminal probe hybridized to a 1-kb band, also detected by the *neo* probe and representing a fusion of the *neo* transcript and N-terminal annexin A7 sequences (data not shown). These different RNA species were present in all tissues analyzed. We performed also reverse transcription-PCR with different primer pairs for the N-terminal region, the resistance cassette, and the core domain and could amplify a fragment representing an *Anxa7-neo* hybrid sequence composed of the N-terminal part of annexin A7 up to exon 7 and the *neo* cassette. These data indicate that no intact mRNA for annexin A7 was formed in *Anxa7*$^{-/-}$ mice. To verify the absence of annexin A7 protein in homozygous mice, we examined brain, heart, pancreas, and skeletal muscle tissues. Western blot analysis of the tissues was performed by using mouse monoclonal antibodies or polyclonal sera. No annexin A7 protein bands were detected in these tissues in the homozygous mutant mice, whereas strong signals were present in the WT animals (Fig. 1D). Unexpectedly, Western blot analysis of liver homogenates showed a 47-kDa protein in the mutant mice. This protein was detected by several monoclonal antibodies and the polyclonal serum raised against recombinant full-length annexin A7. Further characterization showed grossly different pIs (WT, 5.8; *Anxa7*$^{-/-}$, 8.9) and dissimilar behaviors in an annexin purification scheme (data not shown). It is therefore presumed that this protein is not identical to annexin A7 but rather a liver-specific protein.

Given the absence of a striking phenotype, the possibility that other members of the annexin family might compensate for the loss of annexin A7 was investigated. As such compensation could be reflected in altered gene expression, the levels of annexins A1, A2, A4, A5, A6, and A11, the closest relative to annexin A7, were studied by Western blotting of liver, brain, heart, and skeletal muscle protein from WT and mutant mice. No significant differences in the expression for any of these annexins was detected (Fig. 2). These data were also supported by gene expression studies using DNA microarrays, where significant differences in mRNA levels were also not seen.

To exclude morphological abnormalities in the organs of *Anxa7*$^{-/-}$ mice, we performed histological analysis of brain, heart, kidney, liver, lung, spleen, and skeletal muscle tissues from mutant animals and their littermates at 8 weeks and 10 months of age. None of the organs tested showed obvious abnormalities. More detailed analysis of skeletal muscle using different functional stains also revealed no differences (data not shown).

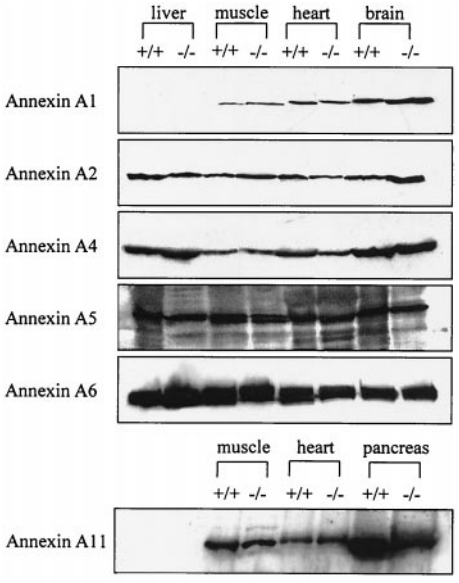

FIG. 2. Expression of annexins in *Anxa7*$^{-/-}$ mice. Proteins from liver, skeletal muscle, heart, and brain were resolved by SDS–12% polyacrylamide gel electrophoresis and transferred to nitrocellulose membranes for Western blotting. In all tissues of the knockout mice, expression patterns of the different annexins were the same as in the WT animals.

Insulin secretion is unaffected in *Anxa7*$^{-/-}$ mice. Insulin secretion is regulated by Ca^{2+}-dependent mechanisms (34). Since it has been suggested that annexin A7 mediates Ca^{2+}- and GTP-induced secretion, we tested the secretory behavior of pancreatic Langerhans islets in *Anxa7*$^{-/-}$ mice. The average insulin contents of 177.2 ± 16.4 ng/islet (n = 7) for WT mice and 171.8 ± 20.7 ng/islet (n = 7) for *Anxa7*$^{-/-}$ mice were not significantly different (Fig. 3A). To investigate the effects of Ca^{2+}, cyclic AMP (cAMP), and metabolism on insulin secretion, isolated islets were stimulated by tolbutamide (100 μM), forskolin (5 μM), and glucose (16.7 mM), respectively. Raising the glucose concentration of the medium from 2 to 16.7 mM increased secretion from islets of WT mice almost sevenfold, and that from islets of *Anxa7*$^{-/-}$ mice ninefold (Fig. 3B). At 2 mM glucose, insulin secretion was not increased by the addition of 5 μM forskolin, while at high glucose (16.7 mM), forskolin potentiated glucose-induced secretion twofold in islets of both WT and knockout mice. Tolbutamide did not increase insulin secretion at 2 mM glucose (Fig. 3B). These results reveal that exocytotic release of insulin stimulated by Ca^{2+} and cAMP is not significantly altered by the absence of annexin A7.

Receptor agonists, which modulate insulin secretion, were then tested. The physiological inhibitor adrenaline (1 μM) inhibited insulin secretion to the same extent in the knockout and WT islets (Fig. 3C). CCh potentiates insulin secretion by activation of phospholipase C, resulting in the generation of diacylglycerol and IP_3. CCh (1 μM) was tested in the presence of glucose (16.7 mM) by perfusion of 100 isolated islets (Fig. 3D). Glucose-induced insulin secretion was augmented by CCh in both WT and *Anxa7*$^{-/-}$ mice, but to a lesser degree in the latter (Fig. 3D). These observations taken with those of

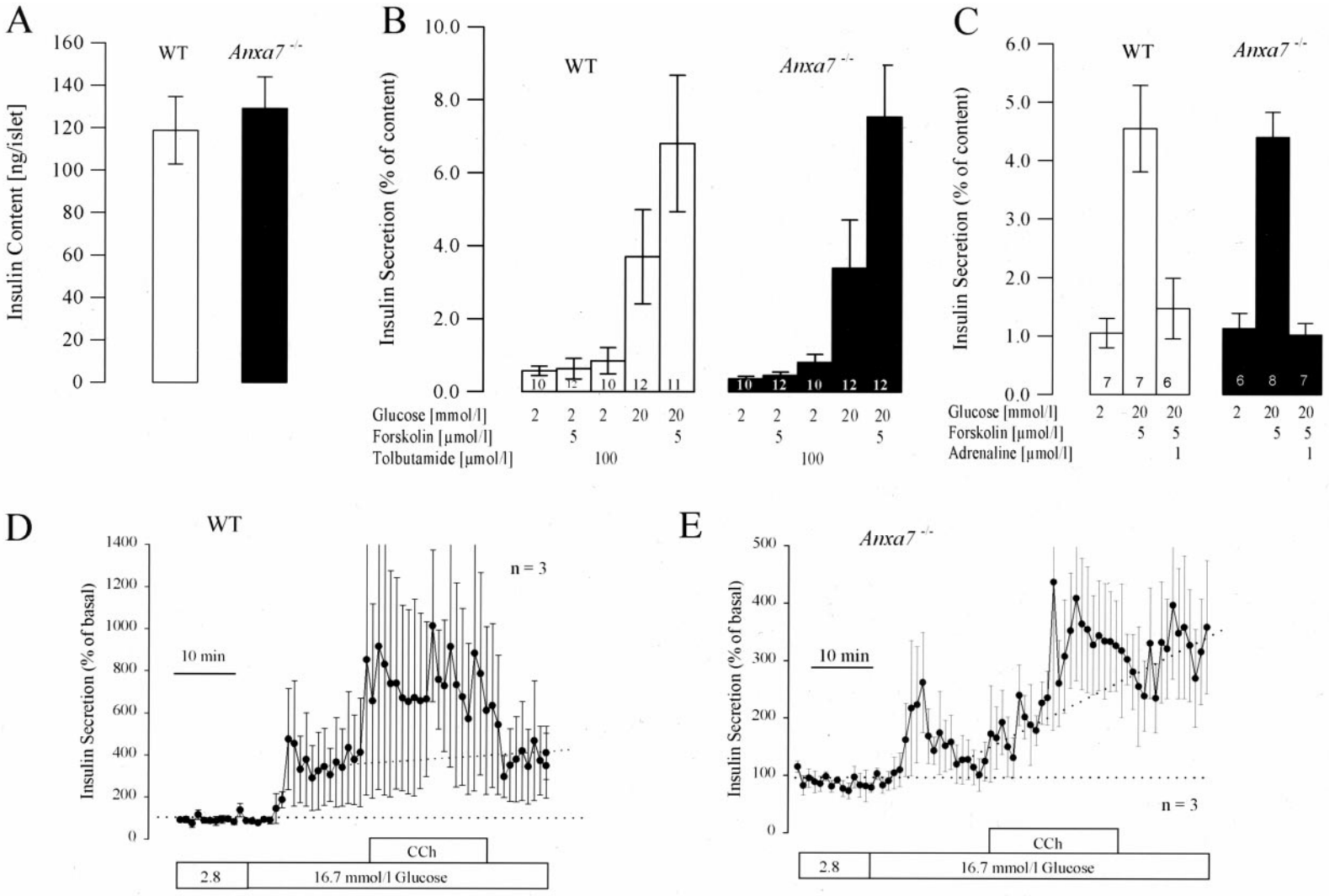

FIG. 3. Insulin secretion in *Anxa7*$^{-/-}$ mice is normal. (A) Insulin content of WT and *Anxa7*$^{-/-}$ islets. Islets were isolated as described in the text, insulin was extracted from 10 islets with acid-ethanol overnight at 4°C, and insulin was measured by radio immuno assay. Results are presented as mean ± SEM for 16 independent determinations. (B) Effects of glucose, forskolin, and tolbutamide on insulin secretion in isolated islets of WT and *Anxa7*$^{-/-}$ mice. Insulin secretion was measured as described above, and substances were added as indicated. Data are presented as mean ± SEM for the number of observations as indicated in each column. (C) Effects of adrenaline on insulin secretion. (D and E) Effects of glucose and CCh in WT (D) and *Anxa7*$^{-/-}$ (E) islets. Perfusion was started with a solution containing 2.8 mM glucose; CCh was added to a concentration of 1 µmol/liter. Data are presented as mean ± SEM from three independent experiments.

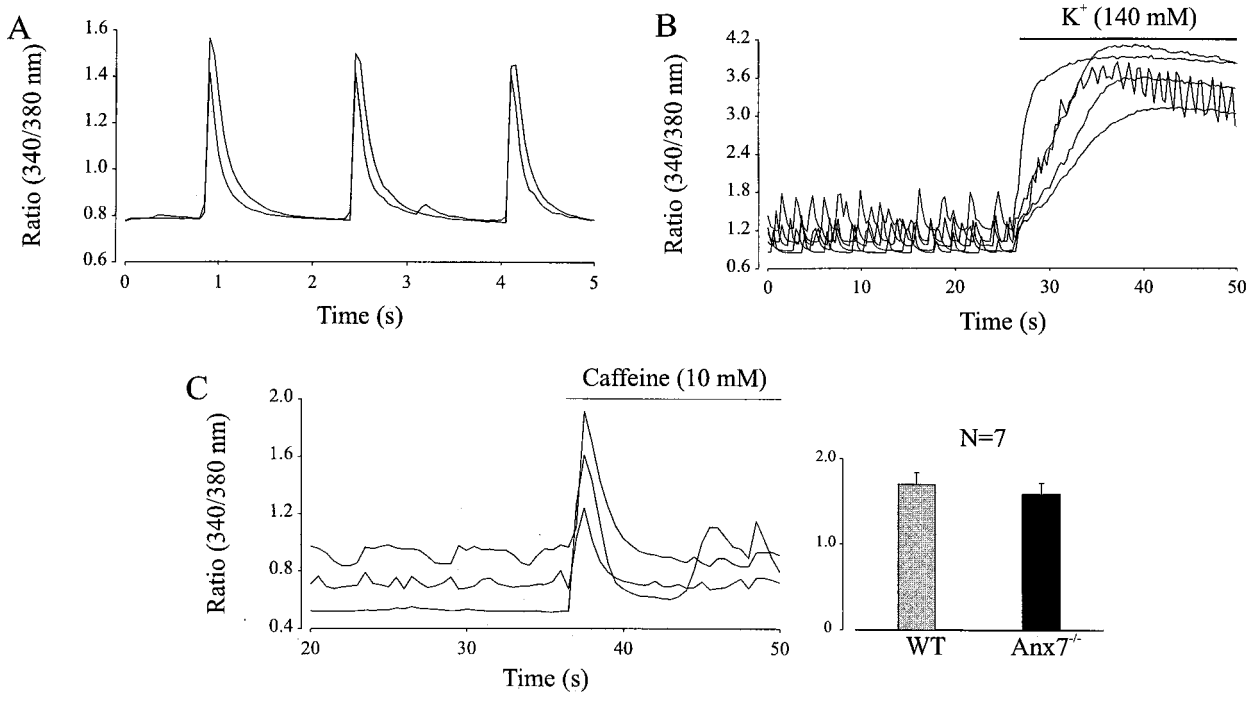

FIG. 4. Ca^{2+} homeostasis in *Anxa7*$^{-/-}$ embryonic cardiomyocytes is intact. (A) Embryonic *Anxa7*$^{-/-}$ cardiomyocytes displayed spontaneous contractile activity accompanied by Ca^{2+} transients. Between the Ca^{2+} transients, stable diastolic Ca^{2+} levels were observed. Changes in Ca^{2+} are displayed as 340/380 nm. (B) Spontaneously beating *Anxa7*$^{-/-}$ embryonic cardiomoycytes responded to depolarization of the membrane potential by elevating the extracellular K^+ concentration with an increase of Ca^{2+}. (C) Extracellular perfusion with the RyR agonist caffeine evoked a transient Ca^{2+} increase in an embryonic *Anxa7*$^{-/-}$ cardiomyocyte. When the increase of the caffeine-induced Ca^{2+} transient was measured in WT and *Anxa7*$^{-/-}$ cardiomyocytes, no significant difference was noted.

Srivastava et al. (39), who described decreased IP_3 receptor number and impaired increases of intracellular Ca^{2+} concentration ($[Ca^{2+}]$) in response to CCh in their *Anxa7*$^{+/-}$ mouse strain, suggest that the diminished secretory response to CCh is due to a decreased number of IP_3 receptors.

Early embryonic cardiomyocytes of *Anxa7*$^{-/-}$ mice display intact Ca^{2+} homeostasis. To address the involvement of annexin A7 in the regulation of cytosolic Ca^{2+}, intracellular Ca^{2+} homeostasis in isolated *Anxa7*$^{-/-}$ cardiomyocytes was analyzed by single-cell imaging techniques. To circumvent compensational effects, the experiments were performed during early embryonic development (E11.5 to E12.5). Embryonic cardiomyocytes are characterized by spontaneous contractions accompanied by intracellular Ca^{2+} transients (41, 45). This feature was also observed in *Anxa7*$^{-/-}$ cardiomyocytes ($n = 30$ derived from three mice) (Fig. 4A). The resting Ca^{2+} (ratio of 0.78 ± 0.02) was of a range similar to that occurring in WT cells (ratio of 0.94 ± 0.02, $n = 16$). Moreover, similar values of peak Ca^{2+} concentration during the spontaneous contractions were observed in *Anxa7*$^{-/-}$ (ratio of 1.28 ± 0.047, $n = 30$) and WT (ratio of 1.63 ± 0.057, $n = 16$) cardiomyocytes, indicating intact excitation-contraction coupling. Because of the important functional role of ryanodine-sensitive Ca^{2+} stores for the heart, their expression was assayed using the ryanodine receptor (RyR) agonist caffeine (10 mM). Caffeine evoked Ca^{2+} transients in the *Anxa7*$^{-/-}$ cardiomyocytes with a similar amplitude (ratio of 1.69 ± 0.132, $n = 7$) as found in WT cells (ratio of 1.7 ± 0.136, $n = 7$; Fig. 4C), supporting intact Ca^{2+} homeostasis and functional expression of ryanodine-sensitive Ca^{2+} stores in *Anxa7*$^{-/-}$ mice.

To study the loss of annexin A7 upon Ca^{2+}-induced Ca^{2+} release (CICR), patch-clamp experiments were performed. *Anxa7*$^{-/-}$ cardiomyocytes displayed normal action potentials (90% action potential duration, 242.7 ± 43.7 [Fig. 5A]) with a maximum diastolic potential of 56.8 ± 1.7 mV ($n = 7$), suggesting the functional expression of cardiac ion channels. This was corroborated by voltage-clamp experiments, where using ramp depolarizations (from -100 to 50 mV, 150 ms) inward rectifier (I_{Kt}), Na^+, and Ca^{2+} as well as outward rectifier K^+ currents could be detected (Fig. 5B, $n = 6$). Because of the critical role of L-type I_{Ca} for heart function, their expression and hormonal modulation were also analyzed. I_{Ca} densities evoked by 50-ms lasting depolarizing voltage steps from an HP of -50 to 0 mV were found to be similar in *Anxa7*$^{-/-}$ cardiomyocytes (14.1 ± 2.5 pA/pF, $n = 7$ [Fig. 5C]) and WT cells (17.4 ± 2 pA/pF, $n = 7$). In line with a normal buildup of intracellular signaling cascades at the early embryonic stage (20), the muscarinergic agonist CCh (1 μM) depressed basal I_{Ca} by $51.7 \pm 8\%$ ($n = 3$) in *Anxa7*$^{-/-}$ cardiomyocytes and by $47.3 \pm 6\%$ ($n = 3$) in WT cardiomyocytes. This could also be observed in current-clamp experiments, where application of CCh resulted in a pronounced negative chronotropic effect, reversible upon washout (Fig. 5D and E, $n = 4$). The CCh action was not accompanied by hyperpolarization of the membrane potential, suggesting the effect of CCh to be related to depression of I_{Ca} (21). Taken together, these data demonstrate

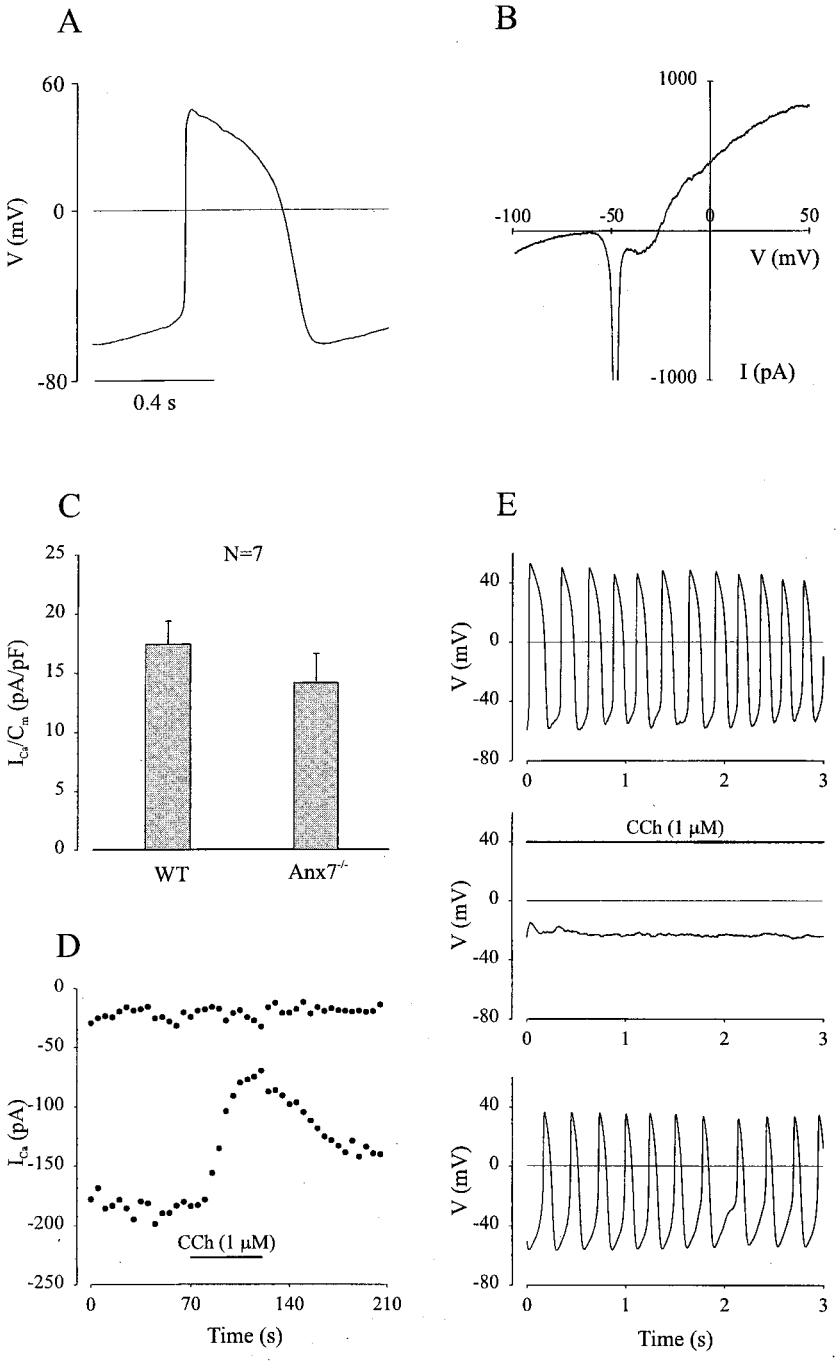

FIG. 5. Normal electrophysiological characteristics are found in *Anxa7*$^{-/-}$ embryonic cardiomyocytes. (A) An early embryonic, spontaneously contracting *Anxa7*$^{-/-}$ ventricular cardiomyocyte displayed a typical ventricular action potential. (B) By applying a 150-ms ramp depolarization from −100 to 50 mV, the functional expression of I_{Kl}, I_{Na}, I_{Ca} and I_{Kout} was detected. (C) The current densities of I_{Ca} were similar in WT and *Anxa7*$^{-/-}$ cardiomyocytes. (D) A representative *Anxa7*$^{-/-}$ embryonic cardiomyocyte responded to CCh application with a prominent depression of basal I_{Ca}, which could be reversed by washout. (E) CCh addition to a spontaneously contracting *Anxa7*$^{-/-}$ early embryonic ventricular cardiomyocyte led to a halt of the electrical activity, accompanied by a small depolarization of the membrane potential. The effect of CCh could be reversed by washout.

that the components required for EC coupling and its hormonal modulation are expressed in *Anxa7*$^{-/-}$ embryonic cardiomyocytes.

Shortening-frequency relationship is altered in *Anxa7*$^{-/-}$ mice. The failure to observe aberrations in the embryonic cardiomyocytes of *Anxa7*$^{-/-}$ mice does not rule out changes in cells from adult hearts, where mechanical and electrophysiological stress is increased and the mechanisms for excitation-contraction more differentiated. In particular, the T-tubular system is highly developed in the adult cardiomyocyte. In most

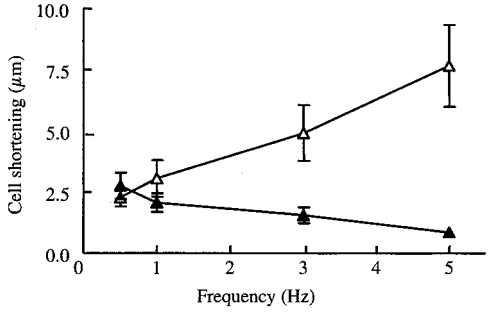

FIG. 6. Shortening-frequency relationship measured in single cardiomyocytes from *Anxa7*$^{-/-}$ (filled triangles) and and WT (open triangles) mice. Shortening-frequency relationship was impaired in the *Anxa7*$^{-/-}$ group. $P < 0.05$ versus *Anxa7*$^{-/-}$.

mammalian species, including mice, an increase in the stimulation frequency is accompanied by an increase in the contractile force (4). This is caused partly by a frequency-induced increase in the intracellular systolic Ca^{2+} concentration, possibly through a greater Ca^{2+} release from sarcoplasmic reticulum (37) or by an increased Ca^{2+} influx via I_{Ca} (32). Differences in the regulation of the intracellular Ca^{2+} homeostasis can be examined by measuring changes in cell shortening and diastolic cell length in isolated, ventricular myocytes, electrically stimulated at increasing stimulation frequencies. Under basal conditions (0.5 Hz), maximal cell shortening was 2.3 ± 0.3 μm in *Anxa7*$^{-/-}$ mice ($n = 15$ from three mice) and 1.8 ± 0.2 μm in the control group ($n = 14$ from six mice) (Fig. 6). In controls, cell shortening was increased when the frequency of stimulation was raised from 0.5 to 5 Hz (2.3 ± 0.4 versus 7.7 ± 1.7 μm, $n = 8$ from four mice). In contrast, cell shortening declined at increasing stimulation frequencies in *Anxa7*$^{-/-}$ mice (2.8 ± 0.5 versus 0.9 ± 0.1 μm, $n = 8$ from two mice). Diastolic cell length did not change during the experiments (0.5 versus 5.0 Hz; WT, 129 ± 10 versus 127 ± 10 μm; *Anxa7*$^{-/-}$, 102 ± 10 versus 107 ± 14 μm) (Fig. 6).

To test whether annexin A7 is involved in the positive inotropic effect induced by stimulation of the β-adrenergic receptor/adenylyl cyclase system, concentration responses to isoprenaline (0.1 to 3 μM) were performed in isolated electrically (0.5 Hz) stimulated ventricular myocytes. The maximal isoprenaline-induced increase in cell shortening was not different between *Anxa7*$^{-/-}$ mice and their WT littermates (Table 1). In both groups, diastolic cell length remained stable during the experiments (data not shown).

TABLE 1. Influence of isoprenaline on cell shortening and diastolic cell length in isolated ventricular murine cardiomyocytes from *Anxa7*$^{-/-}$ mice ($n = 5$ from two mice) and controls ($n = 3$ from two mice)

Mice	Maximum Iso[a]-induced cell shortening (μm)	50% effective concn (μmol/liter)	Diastolic cell length (μm)	
			0	Iso (3 μmol/liter)
Anxa7$^{-/-}$	+2.7 ± 0.7[b]	0.031 ± 0.004	74 ± 10	73 ± 10
Controls	+2.6 ± 1.2	0.142 ± 1.29	92 ± 10	86 ± 8

[a] Iso, isoprenaline.
[b] $P < 0.05$ versus basal.

DISCUSSION

The annexin A7 gene is not essential for mouse viability. Although annexin A7 is expressed in almost every tissue and in undifferentiated ES cells (C. Herr, unpublished data), mice lacking this gene are viable, are fertile, and show no severe changes. The results presented here differ from those recently reported (39), where targeted disruption of the *Anxa7*$^{-/-}$ gene resulted in an embryonic lethality, and where heterozygous animals displayed a defect in IP_3 receptor expression, Ca^{2+} signaling, and insulin secretion. The discrepancy could be due to differences in the induced mutations. In the mouse lines described here, the *neo* cassette was inserted directly into exon 8 of the annexin A7 gene, whereas Srivastava et al. replaced part of intron 5 and exon 6, an exon transcribed only in striated muscle and in the brain (39). Further, the *neo* gene was oriented differently in the two strains, being transcribed in the opposite direction to *Anxa7*$^{-/-}$ in the mice described here. Hence, the conflicting results might be due to alterations in the expression of other genes in the vicinity of the integration site, as demonstrated for the myogenic basic helix-loop-helix gene *MRF4* (31), where similar differences occurred in knockout strains. One further variable could be the different genetic backgrounds used, as has been seen for the gelsolin knockout strain, which was viable on a mixed background but showed almost 100% lethality when bred on a BALB/c or C57BL/6 background (23). It should be noted that the *Anxa7*$^{-/-}$ mutation presented here has been bred on 129SV and C57BL/6 backgrounds without a loss in viability (Herr, unpublished data).

Having generated viable annexin A7-deficient mice, we could address questions relating to annexin A7 function. Striated muscle was studied to reveal effects due to altered Ca^{2+} homeostasis, while Langerhans islets were used as a test system for the analysis of secretion. Overall, no obvious defects caused by the loss of annexin A7 in the mice were observed. At a cellular level, previous experiments suggested that annexin A7 is required as a Ca^{2+}/GTPase in secretion events, as a Ca^{2+} ion channel, or as an ion channel regulator. We now conclude that annexin A7 is not crucial for these events. Our results do not, however, preclude it having a modulatory role in exocytosis or secretion or in regulating Ca^{2+} homeostasis. It should be noted that while the annexin A6-deficient mouse also showed no obvious phenotype (16), overexpression of this protein in the cardiomyocytes of transgenic mice led to cardiomyopathy and heart failure (15), suggesting that annexins can play important modulatory roles. Hence, the lack of an overt phenotype in the absence of annexin A7 could reflect a subtle function; it is also possible that another member of the 10 known murine annexins could compensate for its absence. However, in brain, heart, liver, and skeletal muscle, none of the annexins A1, A2, A4, A5, A6, and A11 were obviously up- or down-regulated at either the mRNA or protein level.

Annexin A7 is not required for insulin secretion. Annexin A7 binds to phospholipids and hydrolyzes GTP in a Ca^{2+}-dependent manner (33). It also promotes membrane aggregation in vitro, a prerequisite for exocytotic membrane fusion (5). Ca^{2+}- and GTP-dependent secretion has been described in a variety of endocrine cells, including chromaffin cells and insulin-secreting β cells (3, 43). These findings suggested a regu-

latory role for annexin A7 during the exocytotics in endocrine cells. However, here we show that annexin A7 is not essential for this process in insulin-secreting cells, since the maximal insulin release was not significantly different from that in the islets of *Anxa7*$^{-/-}$ mice compared to WT mice. Also, the mechanisms for the modulation of exocytosis were not impaired, as in both WT and *Anxa7*$^{-/-}$ islets, the adrenalin response was induced by the interaction of the hormone directly with the exocytotic fusion machinery as well as through lowering cAMP and $[Ca^{2+}]_i$ (42). Further, the insulin content of isolated islets was not significantly different in the *Anxa7*$^{-/-}$ mice compared to WT littermate controls. In contrast, Srivastava et al. observed a 10-fold-larger insulin content and hyperplastic islets in their *Anxa7*$^{+/-}$ mutant mice.

To examine the role of annexin A7 during IP_3-induced mobilization of Ca^{2+}, the effect of CCh on insulin secretion was assessed in *Anxa7*$^{-/-}$ islet cells. CCh-induced secretion was diminished but not abolished in knockout islets. In the *Anxa7*$^{+/-}$ mice of Srivastava et al., 10-fold fewer IP_3 receptors were present, and this was accompanied by a lower and slower increase in $[Ca^{2+}]_i$ compared to islets isolated from WT mice. This loss of IP_3 receptors could be responsible for the impaired release induced by CCh. Indeed, the absence of the IP_3 receptor in mice leads to an unresponsiveness to agonists acting through phospholipase C (40). As IP_3 receptors have been found on secretory vesicles as well as IP_3-sensitive endoplasmic reticular membranes (47), their interaction with annexin A7 may occur at the secretory vesicles. Thus, IP_3-induced Ca^{2+} release may promote annexin A7-mediated membrane aggregation and fusion. Other members of the annexin family are found in rat β cells; for instance, annexin A1 is located on the membrane of insulin-containing granules and maybe involved in the regulation of glucose-induced insulin secretion (29, 30), an event which seems unaffected by the loss of annexin A7. Recently it was suggested that annexin A11 plays a role in Ca^{2+}- or GTPγS-induced insulin secretion (19) and therefore may compensate for the loss of annexin A7. However, there was no alteration in the levels of annexin A11 in the mutant mice.

Is annexin A7 involved in Ca^{2+} homeostasis of cardiomyocytes? The studies with early embryonic cardiomyocytes clearly indicate intact Ca^{2+} homeostasis and expression of the cellular components required for CICR; however, adult *Anxa7*$^{-/-}$ cardiomyocytes exhibited a decrease in frequency-induced cell shortening. This implies that the regulation of electromechanical coupling at high systolic Ca^{2+} concentration is impaired and indicates that annexin A7 is involved in the regulation of Ca^{2+} homeostasis and/or the function of the contractile apparatus in the adult stage. The defect does not, however, interfere with the viability of animals maintained under normal conditions.

While a direct interaction between annexin A7 and myofilaments has not been reported, it was shown recently that annexin A7 binds in a Ca^{2+}-dependent manner to sorcin, a protein which functionally interacts with the Ca^{2+} release channel of the sarcoplasmic reticulum (RyR) (44). Like annexin A7, sorcin translocates from the cytoplasm to the membrane with increasing intracellular Ca^{2+} concentrations, and annexin A7 may recruit sorcin to the plasma membrane (6, 27). Sorcin has been suggested to mediate interchannel communication between the L-type Ca^{2+} channels on the plasma membrane and RyR protein at the sarcoplasmic reticulum during excitation-contraction coupling in the postnatal cardiac muscle (25, 26). This possibly explains the intact function of embryonic cardiomyocytes lacking annexin A7, as the contractile machinery in the immature rodent heart is activated largely by Ca^{2+} entering the cell directly through L-type channels rather than by RyR-mediated CICR (2, 7). As the T-tubule/sarcoplasmic reticulum system gradually develops, contraction becomes more dependent on CICR (7); hence, the decrease in cell shortening seen upon high-frequency stimulation in the cardiomyocytes of adult *Anxa7*$^{-/-}$ mice may result from impairment of the interaction between sorcin and RyR. Annexin A7's localization at the T-tubule system makes it well suited to modulate such an interaction (38).

ACKNOWLEDGMENTS

We thank Stephan Selbert, Olaf Weiner, Regine Brokamp, and Jana Köhler for help during the initial phase of this project, Andrea Hufschmidt, Berthold Gassen, and Rolf Müller for skilled technical help, Volker Gerke, Mitsumori Kawaminami, Walther van Venrooij, and Carlotta Zamparelli for providing reagents, Walter Witke for the genomic library, and Michael Schleicher for discussion.

S.U. is a recipient of a Heisenberg fellowship. This work was supported by grants from the DFG and the Center for Molecular Medicine Cologne to A.A.N.

REFERENCES

1. **Ali, S. M., M. J. Geisow, and R. D. Burgoyne.** 1989. A role for calpactin in calcium-dependent exocytosis in adrenal chromaffin cells. Nature **340:**313–315.
2. **Bers, D. M., L. Li, H. Satoh, and E. McCall.** 1998. Factors that control sarcoplasmic reticulum calcium release in intact ventricular myocytes. Ann. N. Y. Acad. Sci. **853:**157–177.
3. **Bittner, M. A., R. W. Holz, and R. R. Neubig.** 1986. Guanine nucleotide effects on catecholamine secretion from digitonin-permeabilized adrenal chromaffin cells. J. Biol. Chem. **261:**10182–10188.
4. **Bowditch, H. P.** 1871. Über die Eigenthümlichkeit en der Reizbarkeit, welche die Muskelfasern des Herzens zeigen. Ber. Verh. Saechs. Ges. (Akad.) Wiss. **23:**652–689.
5. **Caohuy, H., M. Srivastava, and H. B. Pollard.** 1996. Membrane fusion protein synexin (annexin 7) as a Ca2+/GTP sensor in exocytotic secretion. Proc. Natl. Acad. Sci. USA **93:**10797–10802.
6. **Clemen, C. S., A. Hofmann, C. Zamparelli, and A. A. Noegel.** 1999. Expression and localisation of annexin 7 (synexin) isoforms in differentiating myoblasts. J. Muscle Res. Cell Motil. **20:**669–679.
7. **Cohen, N. M., and W. J. Lederer.** 1988. Changes in the calcium current of rat heart ventricular myocytes during development. J. Physiol. (London) **406:**115–146.
8. **Creutz, C. E., C. J. Pazoles, and H. B. Pollard.** 1978. Identification and purification of an adrenal medullary protein (synexin) that causes calcium-dependent aggregation of isolated chromaffin granules. J. Biol. Chem. **253:**2858–2866.
9. **Doetschman, T. C., H. Eistetter, M. Katz, W. Schmidt, and R. Kemler.** 1985. The in vitro development of blastocyst-derived embryonic stem cell lines: formation of visceral yolk sac, blood islands and myocardium. J. Embryol. Exp. Morphol. **87:**27–45.
10. **Drust, D. S., and C. E. Creutz.** 1988. Aggregation of chromaffin granules by calpactin at micromolar levels of calcium. Nature **331:**88–91.
11. **Emans, N., J. P. Gorvel, C. Walter, V. Gerke, R. Kellner, G. Griffiths, and J. Gruenberg.** 1993. Annexin II is a major component of fusogenic endosomal vesicles. J. Cell Biol. **120:**1357–1369.
12. **Fleischmann, M., W. Bloch, E. Kolossov, C. Andressen, M. Muller, G. Brem, J. Hescheler, K. Addicks, and B. K. Fleischmann.** 1998. Cardiac specific expression of the green fluorescent protein during early murine embryonic development. FEBS Lett. **440:**370–376.
13. **Glenney, J. R., Jr.** 1987. Calpactins: calcium-regulated membrane-skeletal proteins. Biochem. Soc. Trans. **15:**798–800.
14. **Görg, A.** 1993. Two-dimensional electrophoresis with immobilized pH gradients: current state. Biochem. Soc. Trans. **21:**130–132.
15. **Gunteski-Hamblin, A. M., G. Song, R. A. Walsh, M. Frenzke, G. P. Boivin, G. W. Dorn, 2nd, M. A. Kaetzel, N. D. Horseman, and J. R. Dedman.** 1996. Annexin VI overexpression targeted to heart alters cardiomyocyte function. Am. J. Physiol. **270:**H1091–H1100.

16. **Hawkins, T. E., J. Roes, D. Rees, J. Monkhouse, and S. E. Moss.** 1999. Immunological development and cardiovascular function are normal in annexin VI null mutant mice. Mol. Cell. Biol. **19:**8028–8032.
17. **Hoischen, S., K. Brixius, and R. H. Schwinger.** 1998. T- and L-type Ca2+-channel antagonists reduce contractility in guinea pig cardiac myocytes. J. Cardiovasc. Pharmacol. **32:**323–330.
18. **Huber, R., J. Römisch, and E. P. Paques.** 1990. The crystal and molecular structure of human annexin V, an anticoagulant that binds to calcium and membranes. EMBO J. **9:**3867–3874.
19. **Iino, S., T. Sudo, T. Niwa, T. Fukasawa, H. Hidaka, and I. Niki.** 2000. Annexin XI may be involved in Ca2+- or GTPγS-induced insulin secretion in the pancreatic beta-cell. FEBS Lett. **479:**46–50.
20. **Ji, G. J., B. K. Fleischmann, W. Bloch, M. Feelisch, C. Andressen, K. Addicks, and J. Hescheler.** 1999. Regulation of the L-type Ca2+ channel during cardiomyogenesis: switch from NO to adenylyl cyclase-mediated inhibition. FASEB J. **13:**313–324.
21. **Kolossov, E., B. K. Fleischmann, Q. Liu, W. Bloch, S. Viatchenko-Karpinski, O. Manzke, G. J. Ji, H. Bohlen, K. Addicks, and J. Hescheler.** 1998. Functional characteristics of ES cell-derived cardiac precursor cells identified by tissue-specific expression of the green fluorescent protein. J. Cell Biol. **143:** 2045–2056.
22. **Kuijpers, G. A., G. Lee, and H. B. Pollard.** 1992. Immunolocalization of synexin (annexin 7) in adrenal chromaffin granules and chromaffin cells: evidence for a dynamic role in the secretory process. Cell Tissue Res. **269:** 323–330.
23. **Kwiatkowski, D. J.** 1999. Functions of gelsolin: motility, signaling, apoptosis, cancer. Curr. Opin. Cell Biol. **11:**103–108.
24. **Magendzo, K., A. Shirvan, C. Cultraro, M. Srivastava, H. B. Pollard, and A. L. Burns.** 1991. Alternative splicing of human synexin mRNA in brain, cardiac, and skeletal muscle alters the unique N-terminal domain. J. Biol. Chem. **266:**3228–3232.
25. **Meyers, M. B., T. S. Puri, A. J. Chien, T. Gao, P. H. Hsu, M. M. Hosey, and G. I. Fishman.** 1998. Sorcin associates with the pore-forming subunit of voltage-dependent L-type Ca2+ channels. J. Biol. Chem. **273:**18930–18935.
26. **Meyers, M. B., T. S. Puri, A. J. Chien, T. Gao, P. H. Hsu, M. M. Hosey, and G. I. Fishman.** 1998. Sorcin associates with the pore-forming subunit of voltage-dependent L-type Ca2+ channels. J. Biol. Chem. **273:**18930–18935.
27. **Meyers, M. B., C. Zamparelli, D. Verzili, A. P. Dicker, T. J. Blanck, and E. Chiancone.** 1995. Calcium-dependent translocation of sorcin to membranes: functional relevance in contractile tissue. FEBS Lett. **357:**230–234.
28. **O'Farrell, P. H.** 1975. High resolution two-dimensional electrophoresis of proteins. J. Biol. Chem. **250:**4007–4021.
29. **Ohnishi, M., M. Tokuda, T. Masaki, T. Fujimura, Y. Tai, T. Itano, H. Matsui, T. Ishida, R. Konishi, J. Takahara, et al.** 1995. Involvement of annexin-I in glucose-induced insulin secretion in rat pancreatic islets. Endocrinology **136:**2421–2426.
30. **Ohnishi, M., M. Tokuda, T. Masaki, T. Fujimura, Y. Tai, H. Matsui, T. Itano, T. Ishida, J. Takahara, R. Konishi, et al.** 1994. Changes in annexin I and II levels during the postnatal development of rat pancreatic islets. J. Cell Sci. **107:**2117–2125.
31. **Olson, E. N., H. H. Arnold, P. W. Rigby and B. J. Wold.** 1996. Know your neighbors: three phenotypes in null mutants of the myogenic bHLH gene MRF4. Cell **85:**1–4.
32. **Piot, C., S. Lemaire, B. Albat, J. Seguin, J. Nargeot, and S. Richard.** 1996. High frequency-induced upregulation of human cardiac calcium currents. Circulation **93:**120–128.
33. **Pollard, H. B., H. Caohuy, A. P. Minton, and M. Srivastava.** 1998. Synexin (annexin 7) hypothesis for Ca2+/GTP-regulated exocytosis. Adv. Pharmacol. **42:**81–87.
34. **Prentki, M., and F. M. Matschinsky.** 1987. Ca2+, cAMP, and phospholipid-derived messengers in coupling mechanisms of insulin secretion. Physiol. Rev. **67:**1185–1248.
35. **Raynal, P., and H. B. Pollard.** 1994. Annexins: the problem of assessing the biological role for a gene family. Biochim. Biophys. Acta **1197:**63–93.
36. **Russo-Marie, F.** 1992. Macrophages and the glucocorticoids. J. Neuroimmunol. **40:**281–286.
37. **Schwinger, R. H., K. Brixius, U. Bavendiek, S. Hoischen, J. Muller-Ehmsen, B. Bolck, and E. Erdmann.** 1997. Effect of cyclopiazonic acid on the force-frequency relationship in human nonfailing myocardium. J. Pharmacol. Exp. Ther. **283:**286–292.
38. **Selbert, S., P. Fischer, D. Pongratz, M. Stewart, and A. A. Noegel.** 1995. Expression and localization of annexin 7 (synexin) in muscle cells. J. Cell Sci. **108:**85–95.
39. **Srivastava, M., I. Atwater, M. Glasman, X. Leighton, G. Goping, H. Caohuy, G. Miller, J. Pichel, H. Westphal, D. Mears, E. Rojas, and H. B. Pollard.** 1999. Defects in inositol 1,4,5-trisphosphate receptor expression. Ca(2+) signaling, and insulin secretion in the *Anxa7*(+/−) knockout mouse. Proc. Natl. Acad. Sci. USA **96:**13783–13788.
40. **Suzuki, H., H. Takano, Y. Yamamoto, T. Komuro, M. Saito, K. Kato, and K. Mikoshiba.** 2000. Properties of gastric smooth muscles obtained from mice which lack inositol trisphosphate receptor. J. Physiol. (London) **525:**105–111.
41. **Takeshima, H., S. Komazaki, K. Hirose, M. Nishi, T. Noda, and M. Iino.** 1998. Embryonic lethality and abnormal cardiac myocytes in mice lacking ryanodine receptor type 2. EMBO J. **17:**3309–3316.
42. **Ullrich, S., and C. B. Wollheim.** 1988. GTP-dependent inhibition of insulin secretion by epinephrine in permeabilized RINm5F cells. Lack of correlation between insulin secretion and cyclic AMP levels. J. Biol. Chem. **263:**8615–8620.
43. **Vallar, L., T. J. Biden, and C. B. Wollheim.** 1987. Guanine nucleotides induce Ca2+-independent insulin secretion from permeabilized RINm5F cells. J. Biol. Chem. **262:**5049–5056.
44. **Verzili, D., C. Zamparelli, B. Mattei, A. A. Noegel, and E. Chiancone.** 2000. The sorcin-annexin 7 calcium-dependent interaction requires the sorcin N-terminal domain. FEBS Lett. **471:**197–200.
45. **Viatchenko-Karpinski, S., B. K. Fleischmann, Q. Liu, H. Sauer, O. Gryshchenko, G. J. Ji, and J. Hescheler.** 1999. Intracellular Ca2+ oscillations drive spontaneous contractions in cardiomyocytes during early development. Proc. Natl. Acad. Sci. USA **96:**8259–8264.
46. **Witke, W., A. H. Sharpe, J. H. Hartwig, T. Azuma, T. P. Stossel, and D. J. Kwiatkowski.** 1995. Hemostatic, inflammatory, and fibroblast responses are blunted in mice lacking gelsolin. Cell **81:**41–51.
47. **Yoo, S. H., and C. J. Jeon.** 2000. Inositol 1,4,5-trisphosphate receptor/Ca2+ channel modulatory role of chromogranin A, a Ca2+ storage protein of secretory granules. J. Biol. Chem. **275:**15067–15073.
48. **Yoshizaki, H., S. Tanabe, K. Arai, A. Murakami, Y. Wada, M. Ohkuchi, Y. Hashimoto, and M. Maki.** 1992. Effects of calphobindin II (annexin VI) on procoagulant and anticoagulant activities of cultured endothelial cells. Chem. Pharm. Bull. (Tokyo) **40:**1860–1863.